

# Characterization of the Cytochrome *c* Membrane-Binding Site Using Cardiolipin-Containing Bicelles with NMR

Hisashi Kobayashi, Satoshi Nagao,\* and Shun Hirota\*

**Abstract:** Cytochrome (cyt) *c* transports electrons from Complex III to Complex IV in mitochondria. Cyt *c* is ordinarily anchored to the mitochondrial membrane through interaction with cardiolipin (CL), however its release into the cytosol initiates apoptosis. The cyt *c* interaction site with CL-containing bicelles was characterized by NMR spectroscopy. Chemical shift perturbations in cyt *c* signals upon interaction with bicelles revealed that a relatively wide region, which includes the A-site, the CXXCH motif, and the N- and C-terminal helices, and contains multiple Lys residues, interacts cooperatively with CL. The specific cyt *c*–CL interaction increased with increasing CL molecules in the bicelles. The location of the cyt *c* interaction site for CL was similar to those for Complex III and Complex IV, thus indicating that cyt *c* recognizes lipids and partner proteins in a similar way. In addition to elucidating the cyt *c* membrane-binding site, these results provide insight into the dynamic aspect of cyt *c* interactions in mitochondria.

Membrane proteins associated with lipid molecules play diverse roles in cells. These roles include immunoreaction in innate immunity,<sup>[1]</sup> transportation of molecules and ions across cell membranes,<sup>[2]</sup> and ATP synthesis in the respiratory chain.<sup>[2b,3]</sup> Lipid molecules serve not only as scaffolds but also as regulatory factors of membrane proteins in biological systems.<sup>[4]</sup> Cytochrome (cyt) *c* is a peripheral membrane protein that shuttles electrons from the cytb<sub>c</sub><sub>1</sub> complex (Complex III) to cyt *c* oxidase (Complex IV) in the respiratory chain.<sup>[5]</sup> Cyt *c* is ordinarily anchored to the inner mitochondrial membrane through binding to cardiolipin (CL), a specific glycerophospholipid.<sup>[6]</sup>

Although there have been many studies on the binding of cyt *c* to CL-containing membranes,<sup>[6,7]</sup> the location of the CL interaction sites of cyt *c* have lacked high resolution. Spherical vesicles comprising amphipathic phospholipids have typically been used as membrane mimetics to elucidate cyt *c*–lipid interactions.<sup>[6,7c–e]</sup> NMR spectroscopy can provide detailed structural information on the interactions of proteins with other molecules.<sup>[8]</sup> However, for protein/vesicle systems, the tumbling motion of the protein is slowed by binding to the vesicles, which causes signal broadening in solution because the molecular weights of the vesicles are well above the

molecular-weight limit of NMR signal detection for conventional structural characterization (about 100 kDa).<sup>[9]</sup> Small detergent micelles have been used for the characterization of protein–lipid interactions by solution NMR spectroscopy, although a conceivable effect of micelle curvature on the protein structure remains a concern.<sup>[8b,10]</sup> Recently, CL-bound cyt *c* was encapsulated into a reversed micelle in organic solvents and characterized by solution NMR spectroscopy, where cyt *c* interacted with membrane mimetics possessing a large negative curvature.<sup>[8e]</sup> Disk-like bicelles are constructed of short- and long-chain lipids, which are separated into rim and bilayer phases, respectively.<sup>[11]</sup> Bicelles have been utilized to obtain structural and functional insights on membrane proteins through combination with solution and solid-state NMR spectroscopy.<sup>[8b,12]</sup> Small bicelles tumble quickly in solution at an NMR time scale, thus allowing solution NMR investigation of the interaction between a peripheral membrane protein and a bicelle containing lipids that interact with the protein. Nanodiscs formed by a mixture of lipids and membrane scaffold proteins have been developed to characterize membrane proteins in an aqueous medium.<sup>[13]</sup> In this study, we used bicelles with a limited number of CL in each bicelle to characterize the interaction of horse cyt *c* with CL by high-resolution solution NMR spectroscopy.

The bicelle structure and size were characterized by <sup>31</sup>P NMR, cryogenic transmission electron microscopy (Cryo-TEM), and dynamic light scattering (DLS). In the <sup>31</sup>P NMR spectra of the bicelles, three narrow signals corresponding to the phosphate groups of 1,2-dihexanoyl-*sn*-glycero-3-phosphocholine (DHPC), 1,2-dimyristoyl-*sn*-glycero-3-phosphocholine (DMPC), and bovine heart CL were observed between –1.0 and 1.0 ppm (Figure 1A). The DHPC and DMPC chemical shifts of the bicelles were similar to those previously reported for DHPC/DMPC bicelles, which exhibit isotropic tumbling motions in solution.<sup>[12b]</sup> The line broadening of the CL signal in the <sup>31</sup>P NMR spectra was similar to that for other signals (Table S1), thus indicating that CL was incorporated into the bicelles. Bicelles of DHPC/DMPC/CL = 1:0.9:0.1, 1.33:0.9:0.1, and 2:0.9:0.1 (molar ratios) were estimated to form *q* = 1, *q* = 0.75, and *q* = 0.5 (ratio of long-chain to short-chain components) bicelles, respectively, by assuming that DHPC forms the rim region whereas DMPC and CL form the lipid-bilayer region. The bicelles contained 10 mol % CL in their lipid-bilayer regions. The linewidths of the <sup>31</sup>P signals in the spectra increased in the order of the *q* value, which corresponds to an increase in bicelle size (Figure 1A). However, the <sup>31</sup>P NMR spectra of the bicelles did not change with the addition of cyt *c*, thus indicating that the bicelles maintained their structures in the presence of cyt *c*

[\*] H. Kobayashi, Dr. S. Nagao, Prof. Dr. S. Hirota  
Graduate School of Materials Science  
Nara Institute of Science and Technology  
8916-5 Takayama, Ikoma, Nara 630-0192 (Japan)  
E-mail: s-nagao@ms.naist.jp  
hirota@ms.naist.jp

Supporting information for this article can be found under:  
<http://dx.doi.org/10.1002/anie.201607419>.

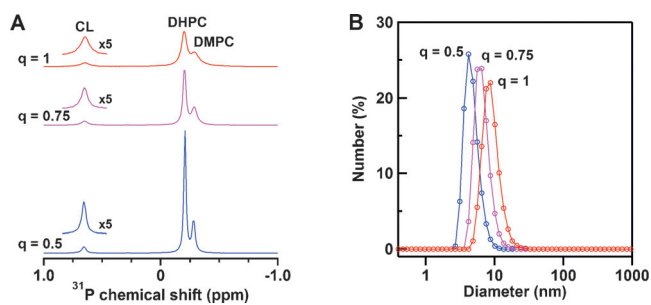


**Figure 1.** A)  $^{31}\text{P}$  NMR spectra and B) DLS size distribution curves of CL-containing bicelles. The spectra and curves for the  $q=1$ ,  $q=0.75$ , and  $q=0.5$  bicelles are shown in red, pink, and blue, respectively. Measurement conditions: solution condition, 25 mM HEPES-NaOH buffer, pH 6.8, containing 50 mM NaCl; [DHPC]=30, 40, and 60 mM for the  $q=1$ ,  $q=0.75$ , and  $q=0.5$  bicelles, respectively; [DMPC]=27 mM; [CL]=3 mM; 25 °C.

(Figure S1 in the Supporting Information). Ellipsoidal objects corresponding to the projections of edge-on discoidal structures were observed in the cryogenic transmission electron microscopy (Cryo-TEM) image of the  $q=1$  bicelles (Figure S2). Average sizes of  $q=1$ ,  $q=0.75$ , and  $q=0.5$  bicelles were estimated by DLS as  $(9.14 \pm 0.81)$  nm,  $(6.74 \pm 0.24)$  nm, and  $(4.73 \pm 0.16)$  nm, with half widths of 2.70 nm, 1.81 nm, and 1.23 nm, respectively (Figure 1B).

$^1\text{H}$  and  $^{15}\text{N}$  signals of the backbone amino acid residues except for Gly1, Glu21, Thr28, Pro30, Gly37, Pro44, Gly45, Thr47, Pro71, Pro76, Gly77, Ala83, Gly84, Lys86, and Lys88 of oxidized wild-type (WT) cyt *c* were assigned, and the chemical shifts of the signals were in good agreement with those reported previously.<sup>[8c,14]</sup>

Solution NMR spectra of oxidized cyt *c* were compared in the presence and absence of CL-containing bicelles to elucidate the interactions between cyt *c* and CL. The line-widths of the  $^1\text{H}$  NMR signals of WT cyt *c* increased slightly upon the addition of  $q=1$  bicelles containing CL (Figure S3B), whereas it did not change upon the addition of  $q=1$  bicelles without CL (Figure S3C). These results indicate that WT cyt *c* interacts with CL in the bicelles. However, in the presence of CL-containing 1,2-dioleoyl-*sn*-glycero-3-phosphocholine (DOPC) vesicles, most of the  $^1\text{H}$  NMR signals of WT cyt *c* were made undetectable by severe signal broadening resulting from the high molecular weight of the vesicles (Figure S3D).

The chemical shift perturbation (CSP) values of Asp2, Lys5, Gly6, Lys7, Lys8, Gln16, Glu61, Glu62, Lys87, and Thr89 of WT cyt *c* upon the addition of CL-containing  $q=1$  bicelles were larger than the average CSP value of all residues for more than the standard deviation (large CSP: CSP value  $\geq 0.014$  ppm; Figures 2 and S4). The CSP values of Val3, Ile9, Gln12, Lys13, Cys17, His18, Thr19, Val20, Gly29, Ala51, Asn54, Asn70, Lys72, Lys73, Tyr74, Phe82, Ile85, Arg91, Asp93, Leu94, Tyr97, and Leu98 were larger than the average CSP value, but within the standard deviation (moderate CSP:  $0.008 \text{ ppm} < \text{CSP value} < 0.014 \text{ ppm}$ ). CSP is caused by a change in the magnetic shielding resulting from contact with other molecules and/or a local protein conformational change.<sup>[8a]</sup> The amino acid residues of cyt *c* in a specific surface

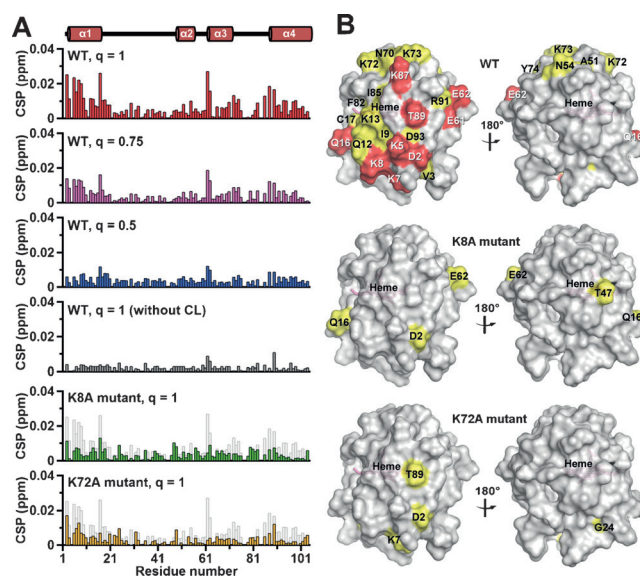


**Figure 2.** CSP values of the amino acid residues and surface mapping of oxidized WT, K8A, and K72A cyt *c* in the presence of CL-containing bicelles. A) The CSP values of backbone signals induced upon interaction with CL. The chemical shift changes of WT cyt *c* for the  $q=1$ ,  $q=0.75$ , and  $q=0.5$  bicelles with CL are shown in red, pink, and blue, respectively. The CSP values of WT cyt *c* for the  $q=1$  bicelle without CL are shown in dark gray. The CSP values of WT cyt *c* are superimposed as light gray bars on those of K8A (green) and K72A (orange) cyt *c*. B) The protein structure (PDB ID: 1AKK) is shown as surface models. The residues with CSP values of  $x < 0.008$ ,  $0.008 \leq x < 0.014$ , and  $0.014 \leq x$  are shown in gray, yellow, and red, respectively. The heme positions are indicated. The left and right figures are rotated horizontally by 180° relative to each other. Measurement conditions: solution condition, 25 mM HEPES-NaOH buffer, pH 6.8, containing 50 mM NaCl; [cyt *c*]=0.3 mM; [DHPC]=30, 40, and 60 mM for the  $q=1$ ,  $q=0.75$ , and  $q=0.5$  bicelles, respectively; [DMPC]=27 mM; [CL]=3 mM;  $[\text{K}_3[\text{Fe}(\text{CN})_6]]$ =0.3 mM; 25 °C.

region containing multiple Lys residues (Lys5, Lys7, Lys8, Lys13, Lys72, Lys73, and Lys87) exhibited large or moderate CSP values, thus revealing that this region is involved in the interaction with CL in the  $q=1$  bicelles (Figure 2B).

The effect of the number of CL molecules in the bicelle on the cyt *c*–CL interaction was investigated with  $q=0.75$  and  $q=0.5$  bicelles containing CL. Although it seems convenient to use  $q=1$  bicelles with different CL/DMPC ratios for elucidation of the effect of CL amount in a bicelle, the preparation of low-CL content bicelles was difficult due to the low solubility of the lipids (e.g., 600 mM of lipids was required for preparation of  $q=1$  bicelles containing 1 mol % CL in the lipid bilayer region). Additionally, aggregates resulted from interaction of cyt *c* with lipids for the  $q=1$  bicelles containing 20 mol % CL in the lipid-bilayer region. Therefore, we constructed  $q=0.75$  and  $q=0.5$  bicelles containing 10 mol % CL in the lipid bilayer regions and varied the number of CL molecules in the bicelle by changing the bicelle size. The number of CL molecules in a bicelle was calculated as 25, 12, and 4 for the  $q=1$ ,  $q=0.75$ , and  $q=0.5$  bicelles, respectively (half of the CL molecules were estimated to exist in each side of the bicelle), assuming a homogenous distribution and using the lipid molecular volumes.<sup>[15]</sup> Although the

CL density of the lipid bilayer was the same among bicelles of different  $q$  values, a cyt *c* molecule may interact with more CL molecules within a bicelle when the bicelle contains more CL molecules (Figure S5). The CSP values of cyt *c* associated with the addition of CL-containing  $q = 0.75$  and  $q = 0.5$  bicelles increased upon increasing the number of CL molecules in the bicelles, although the cyt *c*/CL and CL/DMPC ratios were the same (Figure 2 A and Figure S5). These results show that the specific interaction of cyt *c* with CL becomes stronger with an increase in the number of CL molecules in the bicelles. It is noteworthy that the cyt *c*–CL interaction was weak for the  $q = 0.5$  bicelle, even though the CL density of the bicelle was the same as that of the  $q = 1$  bicelle.

To determine whether the amino acid residues in the specific surface region of cyt *c* interact with CL independently or cooperatively, we separately replaced two positively charged Lys residues that exhibited substantial CSP (Lys8 and Lys72) with Ala (Figure S6)—the two Lys residues were located on the opposite sides of the CL-interaction site (Figure 2 B; distance between the C $_{\beta}$  carbons is ca. 2.6 nm)—and elucidated their effects on the CL-interaction site using the  $q = 1$  bicelle. The CSP values associated with the addition of the  $q = 1$  bicelles containing CL decreased significantly upon replacement of Lys8 or Lys72 (Figure 2). Since Lys8 and Lys72 are relatively distant, these results indicate that the Lys residues in this specific region interact cooperatively with CL.

From the bicelle size and volumes of the lipid compositions, the molecular weights of the bicelles were estimated to be about 300, 150, and 60 kDa for the  $q = 1$ ,  $q = 0.75$ , and  $q = 0.5$  bicelles, respectively.<sup>[15]</sup> Considering that the molecular-weight limit of conventional NMR structural characterization in solution NMR spectroscopy,<sup>[8b]</sup> the high-resolution structural analysis of these bicelles seems difficult. However, the backbone signals of cyt *c* in the presence of CL-containing  $q = 1$  and  $q = 0.75$  bicelles were broadened only slightly in the solution NMR spectra (Figure S3B and Table S1), and the CSP values of the amino acid residues were successfully detected (Figure 2). Under the present cyt *c* and CL-containing bicelle concentrations, it is possible that only a certain amount of cyt *c* molecules exist in the CL-bound state, whereas the rest exist in the free state, and the two states exchange at fast or intermediate time scale during NMR signal detection. Additionally, the high dynamic mobility of the molecules in the bicelle may have contributed to the decrease in the NMR signal linewidths.<sup>[16]</sup>

The structures of membrane proteins and the interaction between membrane proteins and lipids have gained much attention in terms of understanding various biological events. The CL-interaction site of cyt *c* has been proposed from studies using CL-containing vesicles (Figure S7A). For example, the A-site, which contains Lys72, Lys73, Lys86, and Lys87, and the C-site, which contains Asn52, have been reported as a high-affinity electrostatic site<sup>[6b]</sup> and a low-affinity hydrophobic site,<sup>[6a]</sup> respectively. CL binding at the C-site has been suggested to accommodate a hydrophobic channel for the insertion of the CL acyl chain, thereby leading to dissociation of Met80 from the heme iron.<sup>[17]</sup> The L-site, which contains Lys22, Lys25, His26, Lys27, and His33, is an electrostatic interaction site for the acidic phospholipids at low pH, and

membrane fusion is facilitated by the binding at this site.<sup>[7c]</sup> Based on CSP analysis, the A- and L-sites have been reported as the binding sites for reversed-micelles containing CL in organic solvents.<sup>[8c]</sup> In the present study, the A-site was identified as the reversible binding site of cyt *c* in the CL-containing  $q = 1$  bicelles (although no signal was detected for Lys86 in the NMR spectra; Figure 2 B), whereas the C- and L-sites were not identified as interaction sites. When cyt *c* interacted with the CL-containing  $q = 1$  bicelles, Met80 dissociation from the heme iron did not occur, since the Soret band and 695 nm absorption band did not change significantly upon interaction with the bicelles (Figure S8). Given these results, we propose that the interaction of cyt *c* with CL at the A-site is established prior to irreversible binding at the C-site.

In addition to residues at the A-site, residues at the N-terminal helix, the CXXCH motif, and the C-terminal helix (Asp2, Val3, Lys5, Lys7, Lys8, Ile9, Gln12, Lys13, Asn16, Cys17, Ile85, Thr89, Asp93) of horse cyt *c* were included in the interaction site with the CL-containing  $q = 1$  bicelles to form a relatively wide region (Figure 2 B and Figure S7B). Notably, this wide region corresponds well to the cyt *c* interaction site for its redox partners, Complex III<sup>[5c]</sup> and Complex IV<sup>[8a]</sup> (Figure 3). According to the high-resolution structure of iso-1 cyt *c* bound to Complex III revealed by X-ray crystallographic analysis, the residues near the interface of N- and C-terminal helices of iso-1 cyt *c* (Lys11, Thr12, Arg13, Gln16, Lys27, Val28, Ala81, Gly83, Lys86, Lys87, and Lys89, in horse numbering) interact with Complex III.<sup>[5c]</sup> The interaction site of oxidized human cyt *c* for Complex IV has been revealed by solution NMR spectroscopy, where Asp2, Lys5, Ile9, Ile11 (Val in horse cyt *c*), Met12 (Gln in horse cyt *c*), Lys13, Ser15 (Ala in horse cyt *c*), Cys17, His18, Lys79, Met80, Ile81, Val83 (Ala in horse cyt *c*), Lys86, Lys87, Lys88, Glu89 (Thr in horse cyt *c*), Glu90, and Asp93 exhibited large CSP values.<sup>[8a]</sup> The similarity in the location among the interaction sites of cyt *c*

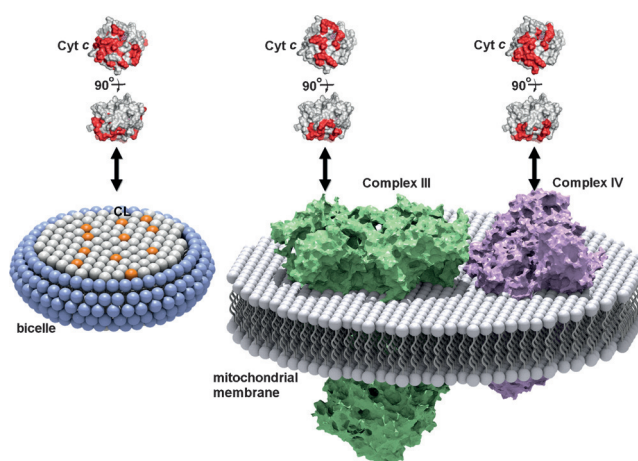


**Figure 3.** Schematic diagram of cyt *c* interaction sites with a CL-containing bicelle, Complex III, and Complex IV. The interaction sites of cyt *c* (PDB ID:1AKK) for CL (present work), Complex III,<sup>[5c]</sup> and Complex IV<sup>[8a]</sup> are shown in red. The head groups of the lipid molecules are shown as sphere models. DHPC, DMPC, and CL molecules in the bicelle are shown in blue, gray, and orange, respectively. Complex III and Complex IV are shown in green and purple, respectively.



for CL, Complex III, and Complex IV reveals that *cyt c* recognizes the lipids and its partner proteins at a similar site, and may exchange its partner through sliding on the inner mitochondrial membrane.

In conclusion, we have identified a relatively wide CL-interaction site on *cyt c* by solution NMR spectroscopy using CL-containing bicelles. The site contains the well-known A-site, N-terminal helix, CXXCH motif, and C-terminal helix, with multiple Lys residues interacting cooperatively with CL. The application of bicelles for the characterization of protein–lipid interaction with high-resolution solution NMR spectroscopy may provide us new insight into not only the detailed interaction sites of peripheral membrane proteins but also their dynamics at the membrane surface.

## Acknowledgements

We thank Ms. Yukie Kitada for preliminary experiments. We are also grateful to Mr. Leigh McDowell (Nara Institute of Science and Technology) for his advice on manuscript preparation. This work was partially supported by Grants-in-Aid from JSPS for Young Scientists (B) (No. JP24750163 (S.N.)) and Scientific Research (B) (No. JP26288080 (S.H.)). This study was also supported by the Green Photonics Project at NAIST sponsored by MEXT.

**Keywords:** bicelles · cytochrome *c* · membrane proteins · protein–lipid interaction · solution NMR

**How to cite:** *Angew. Chem. Int. Ed.* **2016**, *55*, 14019–14022  
*Angew. Chem.* **2016**, *128*, 14225–14228

- [1] C. A. Janeway, Jr., R. Medzhitov, *Annu. Rev. Immunol.* **2002**, *20*, 197–216.
- [2] a) K. S. Ullman, M. A. Powers, D. J. Forbes, *Cell* **1997**, *90*, 967–970; b) K. Faxén, G. Gilderson, P. Ådelroth, P. Brzezinski, *Nature* **2005**, *437*, 286–289; c) A. L. Stouffer, R. Acharya, D. Salom, A. S. Levine, L. Di Costanzo, C. S. Soto, V. Tereshko, V. Nanda, S. Stayrook, W. F. DeGrado, *Nature* **2008**, *451*, 596–599.
- [3] M. Yoshida, E. Muneyuki, T. Hisabori, *Nat. Rev. Mol. Cell Biol.* **2001**, *2*, 669–677.
- [4] a) O. S. Andersen, R. E. Koeppe II, *Annu. Rev. Biophys. Biomol. Struct.* **2007**, *36*, 107–130; b) R. Phillips, T. Ursell, P. Wiggins, P. Sens, *Nature* **2009**, *459*, 379–385.
- [5] a) S. J. Singer, *Annu. Rev. Biochem.* **1974**, *43*, 805–833; b) B. E. Ramirez, B. G. Malmström, J. R. Winkler, H. B. Gray, *Proc. Natl. Acad. Sci. USA* **1995**, *92*, 11949–11951; c) H. Witt, F. Malatesta, F. Nicoletti, M. Brunori, B. Ludwig, *Eur. J. Biochem.* **1998**, *251*, 367–373; d) N. V. Dudkina, H. Eubel, W. Keegstra, E. J. Boekema, H.-P. Braun, *Proc. Natl. Acad. Sci. USA* **2005**, *102*, 3225–3229; e) S. R. N. Solmaz, C. Hunte, *J. Biol. Chem.* **2008**, *283*, 17542–17549; f) T. Althoff, D. J. Mills, J.-L. Popot, W. Kühlbrandt, *EMBO J.* **2011**, *30*, 4652–4664.
- [6] a) M. Rytömaa, P. K. Kinnunen, *J. Biol. Chem.* **1994**, *269*, 1770–1774; b) M. Rytömaa, P. K. Kinnunen, *J. Biol. Chem.* **1995**, *270*, 3197–3202.
- [7] a) M. Ott, J. D. Robertson, V. Gogvadze, B. Zhivotovsky, S. Orrenius, *Proc. Natl. Acad. Sci. USA* **2002**, *99*, 1259–1263; b) V. E. Kagan, V. A. Tyurin, J. Jiang, Y. Y. Tyurina, V. B. Ritov, A. A. Amoscato, A. N. Osipov, N. A. Belikova, A. A. Kapralov, V. Kini, I. I. Vlasova, Q. Zhao, M. Zou, P. Di, D. A. Svistunenko, I. V. Kurnikov, G. G. Borisenko, *Nat. Chem. Biol.* **2005**, *1*, 223–232; c) C. Kawai, F. M. Prado, G. L. Nunes, P. Di Mascio, A. M. Carmona-Ribeiro, I. L. Nantes, *J. Biol. Chem.* **2005**, *280*, 34709–34717; d) N. A. Belikova, Y. A. Vladimirov, A. N. Osipov, A. A. Kapralov, V. A. Tyurin, M. V. Potapovich, L. V. Basova, J. Peterson, I. V. Kurnikov, V. E. Kagan, *Biochemistry* **2006**, *45*, 4998–5009; e) L. V. Basova, I. V. Kurnikov, L. Wang, V. B. Ritov, N. A. Belikova, Vlasova II, A. A. Pacheco, D. E. Winnica, J. Peterson, H. Bayir, D. H. Waldeck, V. E. Kagan, *Biochemistry* **2007**, *46*, 3423–3434; f) P. A. Beales, C. L. Bergstrom, N. Geerts, J. T. Groves, T. K. Vanderlick, *Langmuir* **2011**, *27*, 6107–6115; g) Y. Hong, J. Muenzner, S. K. Grimm, E. V. Pletneva, *J. Am. Chem. Soc.* **2012**, *134*, 18713–18723; h) J. Hanske, J. R. Toffey, A. M. Morenz, A. J. Bonilla, K. H. Schiavoni, E. V. Pletneva, *Proc. Natl. Acad. Sci. USA* **2012**, *109*, 125–130.
- [8] a) K. Sakamoto, M. Kamiya, M. Imai, K. Shinzawa-Itoh, T. Uchida, K. Kawano, S. Yoshikawa, K. Ishimori, *Proc. Natl. Acad. Sci. USA* **2011**, *108*, 12271–12276; b) U. H. N. Dürr, M. Gildenberg, A. Ramamoorthy, *Chem. Rev.* **2012**, *112*, 6054–6074; c) R. E. McGovern, H. Fernandes, A. R. Khan, N. P. Power, P. B. Crowley, *Nat. Chem.* **2012**, *4*, 527–533; d) C. O'Connor, K. L. White, N. Doncescu, T. Didenko, B. L. Roth, G. Czaplinski, R. C. Stevens, K. Wüthrich, A. Milon, *Proc. Natl. Acad. Sci. USA* **2015**, *112*, 11852–11857; e) E. S. O'Brien, N. V. Nucci, B. Fuglestad, C. Tommos, A. J. Wand, *J. Biol. Chem.* **2015**, *290*, 30879–30887; f) A. Mandal, C. L. Hoop, M. DeLucia, R. Kodali, V. E. Kagan, J. Ahn, P. C. A. van der Wel, *Biophys. J.* **2015**, *109*, 1873–1884.
- [9] G. Wang, *Curr. Protein Pept. Sci.* **2008**, *9*, 50–69.
- [10] E. Bárány-Wallje, A. Andersson, A. Gräslund, L. Mäler, *FEBS Lett.* **2004**, *567*, 265–269.
- [11] C. R. Sanders II, G. C. Landis, *Biochemistry* **1995**, *34*, 4030–4040.
- [12] a) K. J. Glover, J. A. Whiles, G. Wu, N. Yu, R. Deems, J. O. Struppe, R. E. Stark, E. A. Komives, R. R. Vold, *Biophys. J.* **2001**, *81*, 2163–2171; b) M. N. Triba, D. E. Warschawski, P. F. Devaux, *Biophys. J.* **2005**, *88*, 1887–1901; c) E. A. Morrison, G. T. DeKoster, S. Dutta, R. Vafabakhsh, M. W. Clarkson, A. Bahl, D. Kern, T. Ha, K. A. Henzler-Wildman, *Nature* **2012**, *481*, 45–50.
- [13] T. H. Bayburt, Y. V. Grinkova, S. G. Sligar, *Nano Lett.* **2002**, *2*, 853–856.
- [14] L. Banci, I. Bertini, H. B. Gray, C. Luchinat, T. Reddig, A. Rosato, P. Turano, *Biochemistry* **1997**, *36*, 9867–9877.
- [15] R. S. Armen, O. D. Uitto, S. E. Feller, *Biophys. J.* **1998**, *75*, 734–744.
- [16] J. Dittmer, L. Thøgersen, J. Underhaug, K. Bertelsen, T. Vosegaard, J. M. Pedersen, B. Schiøtt, E. Tajkhorshid, T. Skrydstrup, N. C. Nielsen, *J. Phys. Chem. B* **2009**, *113*, 6928–6937.
- [17] F. Sinibaldi, B. D. Howes, M. C. Piro, F. Polticelli, C. Bombelli, T. Ferri, M. Coletta, G. Smulevich, R. Santucci, *J. Biol. Inorg. Chem.* **2010**, *15*, 689–700.

Received: August 1, 2016

Revised: September 16, 2016

Published online: October 10, 2016